Accepted Manuscript

A dynamic homogenization model for long-wavelength wave propagation in corrugated sandwich plates

Jia Lou , Jie Yang , Sritawat Kitipornchai , Huaping Wu

Please cite this article as: Jia Lou , Jie Yang , Sritawat Kitipornchai , Huaping Wu , A dynamic homogenization model for long-wavelength wave propagation in corrugated sandwich plates, *International Journal of Mechanical Sciences* (2018), doi: https://doi.org/10.1016/j.ijmecsci.2018.09.033

Highlights

- A dynamic homogenization model is developed for corrugated sandwich plates.

- Analytical solutions are derived for low-frequency dispersion relations.

- The spectral element method is used to validate the homogenization model.

A dynamic homogenization model for long-wavelength wave propagation in corrugated sandwich plates

Jia Lou[1,2], Jie Yang[3,*], Sritawat Kitipornchai[4], Huaping Wu[5]

[1] Department of Mechanics and Engineering Science, Ningbo University, Ningbo, Zhejiang 315211, China

[2] State Key Laboratory for Strength and Vibration of Mechanical Structures, Xi'an Jiaotong University, Xi'an 710049, China

[3] School of Engineering, RMIT University, PO Box 71, Bundoora, VIC 3083, Australia

[4] School of Civil Engineering, The University of Queensland, Brisbane, St Lucia 4072, Australia

[5] Key Laboratory of E&M (Zhejiang University of Technology), Ministry of Education & Zhejiang Province, Hangzhou 310014, China

Abstract

In the present work, a new dynamic homogenization model is developed to investigate the long-wavelength wave propagation in a corrugated sandwich plate. With the harmonic motion assumption and using a shifting operator, the governing equations of the plate are firstly represented in a state-space form. Then, a dynamic homogenization model is developed via the two-scale homogenization method. Based on this model and considering the propagation of sinusoidal waves, the dispersion relations and corresponding wave modes can be easily obtained. In order to validate the developed homogenization model, the obtained dispersion relations are compared with those predicted by the spectral element method. It is found that the present method gives accurate results in low frequency range. Furthermore, the effects of some geometric and material parameters on the dispersion relations for the corrugated sandwich plate are also discussed. The developed homogenization model is expected to be helpful in the prediction and control of dynamic responses of corrugated or even lattice sandwich structures.

Keywords

---

[*] Corresponding author.
E-mail: jie.yang@rmit.edu.au (Jie Yang)

1. Introduction

Sandwich structures, which consist of top and bottom face sheets and a relatively soft core sandwiched between them, have excellent mechanical properties in comparison with traditional solid structures, such as high specific stiffness and high specific strength [1, 2]. Therefore, sandwich structures have wide applications in various fields including aeronautics, astronautics, shipping, and railway [3-5]. The cores of sandwich structures are conventionally made of foams or honeycombs [6]. Comparing with foams and honeycombs, corrugated structures have voids arranged in a specified direction, which enables fluid to flow through the structures, and thus exhibit excellent heat transfer performance [7-9]. Moreover, due to relatively simple manufacturing process, it is a good choice to employ corrugated structures as the cores of lightweight sandwich structures [10]. Recently, some novel corrugated sandwich structures were designed and investigated, such as sandwich structures with multi-layer corrugated cores [11], hierarchical corrugated cores [12], and hybrid honeycomb-corrugated cores [13].

The static and dynamic behaviors of corrugated sandwich structures have been extensively studied. For example, Rubino et al. [14] investigated the quasi-static three-point bending response of corrugated sandwich beams. Cheon and Kim [15] analyzed the mechanical behaviors of corrugated sandwich plates under tensile and bending loads. The energy absorption property and the modal response of corrugated sandwich structures were studied by Zhang et al. [16] and Yang et al. [17], respectively. It is also noted that Wu et al. [18] adopted the spectral element method to analyze the frequency response of corrugated sandwich plates and found that there exists some frequency bands within which the vibration amplitudes are much smaller than those outside these bands.

Wave propagation in plate structures is closely involved with the prediction and control of practical dynamic responses, as well as structural health monitoring (SHM) and non-destructive evaluation/testing (NDE/NDT) [19, 20]. Ultrasonic methods and NDE/NDT techniques are often employed at relatively low frequency, dealing with the onset of the fundamental dispersion branches. In these applications, especially for efficient handling of inverse problems, it is of great importance to know explicit analytical approximations of the long-wavelength dispersion relations. Such estimations are usually tied in with the homogenization concept [21, 22]. It is known that the static and low-frequency vibration behaviors of corrugated sandwich

3

structures may be predicted by a simple equivalent model [23], which considers the sandwich structure as an equivalent structure with a homogenous core. However, due to the discreteness and periodicity of the corrugated core, the wave propagation characteristics of corrugated sandwich structures cannot be accurately described by such a simple equivalent method. Although the above mentioned spectral element method [18] or the finite element method [24, 25] can be used to obtain the whole dispersion relations for corrugated sandwich structures, they could not help to develop a dynamic homogenization model to accurately predict the low-frequency long-wavelength wave propagation behavior. Moreover, in comparison with numerical methods, dynamic homogenization method can provide some physical insights into the long-wavelength wave propagation behavior.

Dynamic homogenization model can be developed based on virtual power principle. For example, Wang and Sun [26] developed a homogenization model including micro-inertia for heterogeneous materials under dynamic loading by using Hamilton's principle. Bathelemy et al. [27] proposed a continuum model via the virtual work principle to described micro-inertia effects in closed-cell foams. Asymptotic expansion provides an alternative approach for developing of dynamic homogenization model. In this respect, Airoldi and Ruzzene [28] considered a one-dimensional metamaterial consisting of a beam and a periodic array of piezoelectric patches, and conducted a homogenization study to illustrate the internal resonant characteristics of the system within an analytical framework. Hui and Oskay [29] developed a nonlocal homogenization model and analyzed the wave dispersion and energy dissipation in biomaterial viscoelastic composites subjected to dynamic loading conditions. Parnell and Abrahams [30] studied the effective response of a periodic fiber reinforced material to SH wave propagation. Chen and Fish [31] developed a dispersive model for wave propagation in periodic heterogeneous media based on higher order homogenization method with multiple spatial and temporal scales. Andrianov et al. [32, 33] studied the wave propagation in linear and nonlinear composite materials by using the higher-order asymptotic homogenization method.

Previous studies have shown that asymptotic homogenization method has been widely employed in the analyses of inhomogeneous elastic materials, including phononic crystals and mechanical metamaterials. Actually, asymptotic homogenization method [34, 35] is a type of multi-scale method, the solution is

4

searched as series expansions in powers of the small parameter $\varepsilon = l/L$ (where l is the typical size of the microstructure, L is the wavelength, and $l << L$). In the present work, a dynamic homogenization model is developed by analytically treating the motion equations of the face sheets and the core sheets of a corrugated sandwich plate and employing a two-scale homogenization procedure, and then applied to analyze the long-wavelength wave propagation behavior of the corrugated sandwich plate. It is known that asymptotic homogenization method could provide a long-wavelength approximation in the low frequency range. While our results show that via taking the microstructural characteristics of the corrugated sandwich structure into consideration and introducing a shifting operator to capture the structural periodicity, the present homogenization yields low-frequency dispersion relations with good accuracy for almost the whole wavenumber range.

The rest of the present paper is structured as follows. In Section 2, a two-scale homogenization model is developed to analyze the long-wavelength wave propagation in a corrugated sandwich plate, and the dispersion relations and corresponding wave modes are calculated. For a comparison study, the dispersion relations based on the spectral element method are also derived. The results predicted by the above two methods are compared in Section 3. Moreover, the effects of some geometric and material parameters on the dispersion relations are also discussed in this section. Finally, some conclusions are drawn in Section 4.

2. Formulation

As shown in Fig.1, an infinite long corrugated sandwich plate with unit width is considered in the present work. The thicknesses of the face sheets and the core sheets are denoted by t_f and t_c, respectively. The length of the core sheets is l_0, and the inclination angle is α.

In Subsection 2.1, a dynamic homogenization model is developed to predict the dispersion relations for the corrugated sandwich plate. In order to validate the present homogenization method, the spectral element method is also presented in Subsection 2.2 to provide the benchmark solutions for the dispersion relations. The results based on these two methods will be compared in Section 3.

2.1 Homogenization method

Fig.1(b) shows a unit cell of the corrugated sandwich plate used for homogenization analysis. The origin of the coordinates is located at the midpoint of

the bottom face sheet. The unit cell consists of four parts, *i.e.*, the top and bottom face sheets, and the left and right core sheets. It is noted that only the motions in the x and y directions are considered in the present work. Since the core of the corrugated sandwich plate is stretching-dominated, it is assumed that the core sheets carry only the axial force, while the face sheets carry both the axial force and the bending moment. Moreover, the mass of each core sheet is taken as two equal concentrated masses respectively located at both ends, which is very similar to the lumped mass method in finite element analyses and expected to be a reasonable approximation in the low-frequency range.

The length of the left core sheet after deformation is denoted by l_l, which can be expressed as:

$$l_l = \sqrt{\left\{l_0 \cos\alpha + \left[u^t(0) - u^b(-l_0\cos\alpha)\right]\right\}^2 + \left\{l_0\sin\alpha + \left[w^t(0) - w^b(-l_0\cos\alpha)\right]\right\}^2}, \quad (1)$$

where the subscript l represents the left core sheet, the superscripts t and b represent the top and bottom face sheets, and u and w are the displacements in the x and y directions, respectively.

In the case of small deformation, by Eq. (1), the elongation of the left core sheet can be approximately written as:

$$\Delta l_l \approx \cos\alpha\left[u^t(0) - u^b(-l_0\cos\alpha)\right] + \sin\alpha\left[w^t(0) - w^b(-l_0\cos\alpha)\right]. \quad (2)$$

Therefore, the magnitude of the axial force in the core sheet is:

$$F_l = \frac{A_c}{l_0}\left\{\cos\alpha\left[u^t(0) - u^b(-l_0\cos\alpha)\right] + \sin\alpha\left[w^t(0) - w^b(-l_0\cos\alpha)\right]\right\}, \quad (3)$$

where $A_c = E_c t_c / (1 - v_c^2)$ is the stretching stiffness of the core sheet, in which E_c and v_c are the Young's modulus and Poisson's ratio of the corrugated core, respectively. The forces applied on the top and bottom face sheets by the left core sheet are denoted by $\mathbf{F}_l^t$ and $\mathbf{F}_l^b$, respectively, whose components can be easily obtained as:

$$F_{lx}^t = -\frac{A_c}{l_0}\left\{\cos^2\alpha\left[u^t(0) - u^b(-l_0\cos\alpha)\right] + \sin\alpha\cos\alpha\left[w^t(0) - w^b(-l_0\cos\alpha)\right]\right\},$$

$$F_{ly}^t = -\frac{A_c}{l_0}\left\{\sin\alpha\cos\alpha\left[u^t(0) - u^b(-l_0\cos\alpha)\right] + \sin^2\alpha\left[w^t(0) - w^b(-l_0\cos\alpha)\right]\right\}, \quad (4)$$

$$F_{lx}^b = -F_{lx}^t, \quad F_{ly}^b = -F_{ly}^t.$$

Similarly, the components of the forces applied on the top and bottom face sheets by the right core sheet can also be obtained:

$$F_{rx}^t = \frac{A_c}{l_0}\left\{\cos^2\alpha\left[u^b(l_0\cos\alpha)-u^t(0)\right]-\sin\alpha\cos\alpha\left[w^b(l_0\cos\alpha)-w^t(0)\right]\right\},$$

$$F_{ry}^t = -\frac{A_c}{l_0}\left\{\sin\alpha\cos\alpha\left[u^b(l_0\cos\alpha)-u^t(0)\right]-\sin^2\alpha\left[w^b(l_0\cos\alpha)-w^t(0)\right]\right\}, \quad (5)$$

$$F_{rx}^b = -F_{rx}^t, \quad F_{ry}^b = -F_{ry}^t.$$

It is known that corrugated sandwich plate is discrete and periodic in the corrugation direction, while continuous and translational invariant in the orthogonal direction. The wave propagation in the corrugation direction is more interesting in comparison with the trivial behavior in the orthogonal direction. Thus, only the wave propagation in the corrugation direction is considered in the present work. Consequently, a special plate theory, in which derivatives in the orthogonal direction are neglected, is adopted here. Moreover, it is assumed that each core sheet carries only axial force and its mass is taken as two equal concentrated masses respectively located at both ends. Therefore, the governing equations for the top and bottom face sheets in the unit cell, respectively, can be expressed as [36]:

$$\left[\rho_f t_f + \rho_c t_c l_0\delta(x)\right]\frac{\partial^2 u^t}{\partial t^2} = A_f\frac{\partial^2 u^t}{\partial x^2} + F_{lx}^t\delta(x) + F_{rx}^t\delta(x),$$

$$\left[\rho_f t_f + \rho_c t_c l_0\delta(x)\right]\frac{\partial^2 w^t}{\partial t^2} + D_f\frac{\partial^4 w^t}{\partial x^4} = F_{ly}^t\delta(x) + F_{ry}^t\delta(x), \quad (6)$$

$$\left[\rho_f t_f + \frac{1}{2}\rho_c t_c l_0\delta(x+l_0\cos\alpha) + \frac{1}{2}\rho_c t_c l_0\delta(x-l_0\cos\alpha)\right]\frac{\partial^2 u^b}{\partial t^2}$$
$$= A_f\frac{\partial^2 u^b}{\partial x^2} + F_{lx}^b\delta(x+l_0\cos\alpha) + F_{rx}^b\delta(x-l_0\cos\alpha),$$

$$\left[\rho_f t_f + \frac{1}{2}\rho_c t_c l_0\delta(x+l_0\cos\alpha) + \frac{1}{2}\rho_c t_c l_0\delta(x-l_0\cos\alpha)\right]\frac{\partial^2 w^b}{\partial t^2}$$
$$+ D_f\frac{\partial^4 w^b}{\partial x^4} = F_{ly}^b\delta(x+l_0\cos\alpha) + F_{ry}^b\delta(x-l_0\cos\alpha). \quad (7)$$

where δ denotes the Dirac delta function, t is the time, ρ_c and ρ_f are the mass density of the corrugated core and the face sheets, $A_f = E_f t_f/(1-v_f^2)$ and $D_f = E_f t_f^3/\left[12(1-v_f^2)\right]$ are the stretching stiffness and bending stiffness of the face sheets, in which E_f and v_f are the Young's modulus and Poisson's ratio of the face sheets, respectively.

7

A shifting operator Δ is defined as follows:

$$\Delta_\alpha u(x) = u(x-\alpha).$$ (8)

By substituting Eqs. (4) and (5) into the governing equations (6) and (7), and using the shifting operator Δ, the governing equations for the top and bottom face sheets in the whole corrugated sandwich plate are obtained as follows:

$$
\left\{\rho_f t_f + \rho_c t_c l_0 \sum_{n=1}^{\infty} \delta\left[x - 2(n-1)l_0\cos\alpha\right]\right\}\frac{\partial^2 u^t}{\partial t^2} = A_f \frac{\partial^2 u^t}{\partial x^2}
$$
$$
-\frac{2A_c}{l_0}\cos^2\alpha \sum_{n=1}^{\infty}\delta\left[x - 2(n-1)l_0\cos\alpha\right]u^t(x)
$$
$$
+\frac{A_c}{l_0}\cos^2\alpha \sum_{n=1}^{\infty}\delta\left[x - 2(n-1)l_0\cos\alpha\right]\left(\Delta_{l_0\cos\alpha} + \Delta_{-l_0\cos\alpha}\right)u^b(x)
$$
$$
+\frac{A_c}{l_0}\sin\alpha\cos\alpha \sum_{n=1}^{\infty}\delta\left[x - 2(n-1)l_0\cos\alpha\right]\left(\Delta_{l_0\cos\alpha} - \Delta_{-l_0\cos\alpha}\right)w^b(x),
$$ (9)

$$
\left\{\rho_f t_f + \rho_c t_c l_0 \sum_{n=1}^{\infty} \delta\left[x - 2(n-1)l_0\cos\alpha\right]\right\}\frac{\partial^2 w^t}{\partial t^2} + D_f \frac{\partial^4 w^t}{\partial x^4}
$$
$$
= \frac{A_c}{l_0}\sin\alpha\cos\alpha \sum_{n=1}^{\infty}\delta\left[x - 2(n-1)l_0\cos\alpha\right]\left(\Delta_{l_0\cos\alpha} - \Delta_{-l_0\cos\alpha}\right)u^b(x)
$$
$$
-\frac{2A_c}{l_0}\sin^2\alpha \sum_{n=1}^{\infty}\delta\left[x - 2(n-1)l_0\cos\alpha\right]w^t(x)
$$
$$
+\frac{A_c}{l_0}\sin^2\alpha \sum_{n=1}^{\infty}\delta\left[x - 2(n-1)l_0\cos\alpha\right]\left(\Delta_{l_0\cos\alpha} + \Delta_{-l_0\cos\alpha}\right)w^b(x),
$$ (10)

$$
\left\{\rho_f t_f + \frac{1}{2}\rho_c t_c l_0 \sum_{n=1}^{\infty} \delta\left[x - (2n-3)l_0\cos\alpha\right] + \frac{1}{2}\rho_c t_c l_0 \sum_{n=1}^{\infty} \delta\left[x - (2n-1)l_0\cos\alpha\right]\right\}\frac{\partial^2 u^b}{\partial t^2}
$$
$$
= A_f \frac{\partial^2 u^b}{\partial x^2} - \frac{A_c}{l_0}\cos^2\alpha \sum_{n=1}^{\infty}\left\{\delta\left[x - (2n-3)l_0\cos\alpha\right] + \delta\left[x - (2n-1)l_0\cos\alpha\right]\right\}u^b(x)
$$
$$
+\frac{A_c}{l_0}\cos^2\alpha \sum_{n=1}^{\infty}\left\{\delta\left[x - (2n-3)l_0\cos\alpha\right]\Delta_{-l_0\cos\alpha} + \delta\left[x - (2n-1)l_0\cos\alpha\right]\Delta_{l_0\cos\alpha}\right\}u^t(x)
$$
$$
-\frac{A_c}{l_0}\sin\alpha\cos\alpha \sum_{n=1}^{\infty}\left\{\delta\left[x - (2n-3)l_0\cos\alpha\right] - \delta\left[x - (2n-1)l_0\cos\alpha\right]\right\}w^b(x)
$$
$$
+\frac{A_c}{l_0}\sin\alpha\cos\alpha \sum_{n=1}^{\infty}\left\{\delta\left[x - (2n-3)l_0\cos\alpha\right]\Delta_{-l_0\cos\alpha} - \delta\left[x - (2n-1)l_0\cos\alpha\right]\Delta_{l_0\cos\alpha}\right\}w^t(x),
$$ (11)

$$\left\{\rho_f t_f + \frac{1}{2}\rho_c t_c l_0 \sum_{n=1}^{\infty}\delta\left[x-(2n-3)l_0\cos\alpha\right] + \frac{1}{2}\rho_c t_c l_0 \sum_{n=1}^{\infty}\delta\left[x-(2n-1)l_0\cos\alpha\right]\right\}\frac{\partial^2 w^b}{\partial t^2}$$

$$+D_f\frac{\partial^4 w^b}{\partial x^4} = -\frac{A_c}{l_0}\sin\alpha\cos\alpha\sum_{n=1}^{\infty}\left\{\delta\left[x-(2n-3)l_0\cos\alpha\right]-\delta\left[x-(2n-1)l_0\cos\alpha\right]\right\}u^b(x)$$

$$+\frac{A_c}{l_0}\sin\alpha\cos\alpha\sum_{n=1}^{\infty}\left\{\delta\left[x-(2n-3)l_0\cos\alpha\right]\Delta_{-l_0\cos\alpha}-\delta\left[x-(2n-1)l_0\cos\alpha\right]\Delta_{l_0\cos\alpha}\right\}u^t(x)$$

$$-\frac{A_c}{l_0}\sin^2\alpha\sum_{n=1}^{\infty}\left\{\delta\left[x-(2n-3)l_0\cos\alpha\right]+\delta\left[x-(2n-1)l_0\cos\alpha\right]\right\}w^b(x)$$

$$+\frac{A_c}{l_0}\sin^2\alpha\sum_{n=1}^{\infty}\left\{\delta\left[x-(2n-3)l_0\cos\alpha\right]\Delta_{-l_0\cos\alpha}+\delta\left[x-(2n-1)l_0\cos\alpha\right]\Delta_{l_0\cos\alpha}\right\}w^t(x),$$

$$(12)$$

in which n represents the n-th unit cell in the longitudinal direction. A state vector is defined as follows:

$$\mathbf{z}^{\varepsilon}(x,t) = \left\{u^t \ P^t \ w^t \ w^t_{,x} \ M^t \ Q^t \ u^b \ P^b \ w^b \ w^b_{,x} \ M^b \ Q^b\right\}^{\mathrm{T}}, \qquad (13)$$

where P, M and Q are respectively the axial force, bending moment and shear force carried by face sheets, the subscript $,x$ denotes the partial derivative with respect to x, and ε represents the dependency of response fields on the microstructure, *i.e.*, the structure within each unit cell. For harmonic motion with frequency ω, $\mathbf{z}^{\varepsilon}(x,t)$ can be expressed as:

$$\mathbf{z}^{\varepsilon}(x,t) = \mathbf{Z}^{\varepsilon}(x)e^{-i\omega t}. \qquad (14)$$

By using Eqs. (9)-(12) and (14), the governing equations can be transformed into the following state-space form:

$$\mathbf{A}(x)\frac{\mathrm{d}}{\mathrm{d}x}\mathbf{Z}^{\varepsilon}(x) = \mathbf{B}^{\varepsilon}(x)\mathbf{Z}^{\varepsilon}(x), \qquad (15)$$

where $\mathbf{A} = \mathrm{diag}\begin{bmatrix} A_f & 1 & 1 & D_f & 1 & 1 & A_f & 1 & 1 & D_f & 1 & 1 \end{bmatrix}$, and the elements of Matrix $\mathbf{B}^{\varepsilon}$ are presented in the Appendix.

Eq. (15) can also be rewritten as:

$$\frac{\mathrm{d}}{\mathrm{d}x}\mathbf{Z}^{\varepsilon}(x) = \mathbf{C}^{\varepsilon}(x)\mathbf{Z}^{\varepsilon}(x), \qquad (16)$$

where $\mathbf{C}^{\varepsilon}(x) = \mathbf{A}^{-1}(x)\mathbf{B}^{\varepsilon}(x)$.

For long-wavelength wave propagation, we develop a two-scale model to describe the problem. Such a method has been widely used in the homogenization of systems with periodically varying properties [28, 37-39]. Introduce a micro-scale

9

variable $s = x/\varepsilon$ (ε is the scaling factor defined as the ratio between the size of the unit cell and the shortest wavelength describing the homogenized response such that $0 < \varepsilon << 1$) to describe the periodicity of the domain, in addition to the macro-scale coordinate x which reflects the long-wavelength behavior. Then, an arbitrary response function, f^{ε}, is expressed using the micro- and macro- scales as $f^{\varepsilon}(x) = f(x, s(x))$. All response fields $f(x, s)$ are assumed to be locally periodic throughout the deformation process:

$$f(x, s) = f(x, s + n\hat{s}),\tag{17}$$

where $\hat{s}$ denotes the period of the microstructure, and n is an arbitrary integer.

The state vector is approximated using an asymptotic expansion with respect to the scaling factor, ε:

$$\mathbf{Z}^{\varepsilon}(x) = \mathbf{Z}(x, s) = \mathbf{Z}^{(0)}(x, s) + \varepsilon\mathbf{Z}^{(1)}(x, s) + \varepsilon^2\mathbf{Z}^{(2)}(x, s) + \cdots,\tag{18}$$

where $\mathbf{Z}^{(0)}$ is the leading order state vector, which will be proven to be independent of micro-scale coordinate s in the following analyses, while the high order state vectors $\mathbf{Z}^{(\alpha)}(\alpha = 1, 2, \cdots)$ are functions of both the macro- and micro-scale coordinates.

Since the considered plate is periodic, the properties depend only on s, therefore,

$$C^{\varepsilon}(x) = C(x, s) = C(s).\tag{19}$$

Accordingly, Eq. (16) can be rewritten as:

$$\frac{\mathrm{d}}{\mathrm{d}x}\mathbf{Z}(x, s) = \mathbf{C}(s)\mathbf{Z}(x, s),\tag{20}$$

in which the derivative can be expressed as:

$$\frac{\mathrm{d}}{\mathrm{d}x} = \frac{\partial}{\partial x} + \frac{1}{\varepsilon}\frac{\partial}{\partial s}.\tag{21}$$

Substituting Eqs. (19) into Eq. (20) yields:

$$\frac{\partial}{\partial x}\mathbf{Z}^{(0)} + \frac{1}{\varepsilon}\frac{\partial}{\partial s}\mathbf{Z}^{(0)} + \varepsilon\frac{\partial}{\partial x}\mathbf{Z}^{(1)} + \frac{\partial}{\partial s}\mathbf{Z}^{(1)} + \varepsilon^2\frac{\partial}{\partial x}\mathbf{Z}^{(2)} + \varepsilon\frac{\partial}{\partial s}\mathbf{Z}^{(2)} + \cdots$$
$$= \mathbf{C}(s)\left(\mathbf{Z}^{(0)} + \varepsilon\mathbf{Z}^{(1)} + \cdots\right),\tag{22}$$

Since ε is arbitrary, the coefficients of each order of ε at both sides of Eq. (22) must be equal. By collecting the coefficients of ε^{-1} and ε^0 in Eq. (22), we have the

following equations:

$$\varepsilon^{-1}: \quad \frac{\partial}{\partial s}\mathbf{Z}^{(0)} = 0, \tag{23}$$

$$\varepsilon^{0}: \quad \frac{\partial}{\partial x}\mathbf{Z}^{(0)} + \frac{\partial}{\partial s}\mathbf{Z}^{(1)} = \mathbf{C}(s)\mathbf{Z}^{(0)}. \tag{24}$$

Eq. (23) implies that

$$\mathbf{Z}^{(0)}(x,s) = \mathbf{Z}^{(0)}(x). \tag{25}$$

Integrating both sides of Eq. (24) with respect to s over one period (from $s = -l_0\cos\alpha/\varepsilon$ to $s = l_0\cos\alpha/\varepsilon$) yields:

$$\frac{\partial}{\partial x}\mathbf{Z}^{(0)} = \mathbf{C}_{\text{hom}}\mathbf{Z}^{(0)}, \tag{26}$$

where

$$\mathbf{C}_{\text{hom}} = \frac{\varepsilon}{2l_0\cos\alpha}\int_{-l_0\cos\alpha/\varepsilon}^{l_0\cos\alpha/\varepsilon}\mathbf{C}(s)\,ds. \tag{27}$$

It is noted that delta functions ($\delta(x)$) do not arise in $\mathbf{C}_{\text{hom}}$ after the integration.

For plane wave propagation, it can be assumed that:

$$\mathbf{Z}^{(0)} = \mathbf{Z}_{\text{m}}^{(0)}e^{i\kappa x}, \tag{28}$$

where κ is the wavenumber. Substituting Eq. (28) into Eq. (26) yields:

$$\left(\bar{\mathbf{C}}_{\text{hom}} - i\kappa\mathbf{I}\right)\mathbf{Z}_{\text{m}}^{(0)} = \mathbf{0}, \tag{29}$$

with the elements of Matrix $\bar{\mathbf{C}}_{\text{hom}}$ being presented in the Appendix. It should be noted that by adopting the assumption expressed by Eq. (28), the shifting operator Δ no longer appears in $\bar{\mathbf{C}}_{\text{hom}}$, so that its elements take much simpler forms. The dispersion relations in the corrugation direction for the corrugated sandwich plate can be obtained by solving the following equation:

$$\det\left(\mathbf{C}_{\text{eq}} - i\kappa\mathbf{I}\right) = 0, \tag{30}$$

which can be also written as:

$$c_1\omega^8 + c_2\omega^6 + c_3\omega^4 + c_4\omega^2 + c_5 = 0. \tag{31}$$

By the above equation, four branches of low-frequency dispersion relations can be predicted, which are expressed as:

$$\omega_{1,2} = \sqrt{-\frac{c_2}{4c_1} - \frac{1}{2}p \pm \frac{1}{2}q}, \quad \omega_{3,4} = \sqrt{-\frac{c_2}{4c_1} + \frac{1}{2}p \pm \frac{1}{2}r}, \tag{32}$$

11

where $\quad p = \sqrt{\dfrac{c_2^2}{4c_1^2} - \dfrac{2c_3}{3c_1} + \Delta}, \quad q = \sqrt{\dfrac{c_2^2}{2c_1^2} - \dfrac{4c_3}{3c_1} - \Delta + \dfrac{(c_2/c_1)^3 - 4c_2c_3/c_1^2 + 8c_4/c_1}{4p}}, \quad$ and

$$r = \sqrt{\dfrac{c_2^2}{2c_1^2} - \dfrac{4c_3}{3c_1} - \Delta - \dfrac{(c_2/c_1)^3 - 4c_2c_3/c_1^2 + 8c_4/c_1}{4p}}. \qquad \text{The} \qquad \text{expressions} \qquad \text{for}$$

$c_i \, (i = 1, 2, \cdots, 5)$ and Δ are given in the Appendix.

2.2 Spectral element method

In this section, the dispersion relations for the corrugated sandwich plate based on the spectral element method are derived. Fig.1(c) shows a unit cell of the corrugated sandwich plate used for spectral element analysis. The origin of the global coordinate system is located at the midpoint of the bottom face sheet, and the origins of two local coordinate systems as depicted in Fig.1(c) are both located at the junction of the core sheets and the top face sheet.

Both the longitudinal and transverse motions of the face sheets are considered. The governing equation for the longitudinal motion reads:

$$A_f u_{j,xx} = \rho_f t_f u_{j,tt} \quad (j = 1,2,3,4), \qquad (33)$$

where the subscript j represents Part j in Fig.1(c). For harmonic motion with frequency ω, the longitudinal displacement $u_j(x,t)$ can expressed as:

$$u_j(x,t) = U_j(x)e^{-i\omega t} \quad (j = 1,2,3,4). \qquad (34)$$

Substituting Eq. (34) into Eq. (33) yields:

$$U_j = A_j \sin k_f x + B_j \cos k_f x \quad (j = 1,2,3,4), \qquad (35)$$

where $k_f = \sqrt{\rho_f t_f / A_f}\,\omega.$

The equation governing the transverse motion of the face sheets reads:

$$D_f w_{j,xxxx} = \rho_f t_f w_{j,tt} \quad (j = 1,2,3,4), \qquad (36)$$

Similarly, the transverse displacement $w_j(x,t)$ can be written as:

$$w_j(x,t) = W_j(x)e^{-i\omega t} \quad (j = 1,2,3,4). \qquad (37)$$

Substituting Eq. (37) into Eq. (36) yields:

$$W_j = C_j \sinh \lambda x + D_j \cosh \lambda x + E_j \sin \lambda x + F_j \cos \lambda x \quad (j = 1,2,3,4), \qquad (38)$$

where $\lambda = \left(\rho_f t_f \omega^2 / D_f\right)^{1/4}.$

Only the longitudinal motion of the core sheets is considered. The corresponding governing equation reads:

$$A_c u_{j,xx} = \rho_c t_c u_{j,tt} \quad (j=5,6),\tag{39}$$

For harmonic motion with frequency ω, the longitudinal displacement $u_j(x,t)$ can also be expressed as:

$$u_j(x,t) = U_j(x)e^{-i\omega t} \quad (j=5,6),\tag{40}$$

Substituting Eq. (40) into Eq. (39) yields:

$$U_j = A_j \sin k_c x + B_j \cos k_c x \quad (j=5,6),\tag{41}$$

where $k_c = \sqrt{\rho_c t_c / A_c}\,\omega.$

The displacements, rotations, axial forces, shear forces and bending moments at the junctions should satisfy the following continuity conditions:

$$\begin{aligned}
&U_1(0) = U_2(0), \ W_1(0) = W_2(0), \ W_1'(0) = W_2'(0), \ M_1(0) = M_2(0),\\
&N_1(0) + \cos\alpha N_5(0) = N_2(0) + \cos\alpha N_6(0),\\
&Q_1(0) - \sin\alpha N_5(0) = Q_2(0) + \sin\alpha N_6(0),\\
&U_3(0) = U_4(0), \ W_3(0) = W_4(0), \ W_3'(0) = W_4'(0),\\
&N_3(0) = N_4(0), \ Q_3(0) = Q_4(0), \ M_3(0) = M_4(0),\\
&U_5(0) = \cos\alpha U_1(0) + \sin\alpha W_1(0), \ U_6(0) = \cos\alpha U_1(0) - \sin\alpha W_1(0),\\
&U_5(-l_0) = \cos\alpha U_3(-l_0\cos\alpha) + \sin\alpha W_3(-l_0\cos\alpha),\\
&U_6(l_0) = \cos\alpha U_4(l_0\cos\alpha) - \sin\alpha W_4(l_0\cos\alpha).
\end{aligned}\tag{42}$$

in which N, Q and M are respectively the axial force, shear force and bending moment, which can be expressed as:

$$N_j(x) = A_f U_j'(x) \ (j=1,2,3,4), \ N_j(x) = A_c U_j'(x) \ (j=5,6),$$

$$Q_j(x) = D_f W_j'''(x) \ (j=1,2,3,4), \ \text{and} \ M_j(x) = D_f W_j''(x) \ (j=1,2,3,4).$$

Moreover, the displacements, rotations, axial forces, shear forces and bending moments at the ends of the unit cell should satisfy the Bloch theorem, *i.e.*:

13

$$U_2\left(l_0\cos\alpha\right)=e^{i\kappa 2l_0\cos\alpha}U_1\left(-l_0\cos\alpha\right),\ W_2\left(l_0\cos\alpha\right)=e^{i\kappa 2l_0\cos\alpha}W_1\left(-l_0\cos\alpha\right),$$

$$W_2'\left(l_0\cos\alpha\right)=e^{i\kappa 2l_0\cos\alpha}W_1'\left(-l_0\cos\alpha\right),\ N_2\left(l_0\cos\alpha\right)=e^{i\kappa 2l_0\cos\alpha}N_1\left(-l_0\cos\alpha\right),$$

$$Q_2\left(l_0\cos\alpha\right)=e^{i\kappa 2l_0\cos\alpha}Q_1\left(-l_0\cos\alpha\right),\ M_2\left(l_0\cos\alpha\right)=e^{i\kappa 2l_0\cos\alpha}M_1\left(-l_0\cos\alpha\right),$$

$$U_4\left(l_0\cos\alpha\right)=e^{i\kappa 2l_0\cos\alpha}U_3\left(-l_0\cos\alpha\right),\ W_4\left(l_0\cos\alpha\right)=e^{i\kappa 2l_0\cos\alpha}W_3\left(-l_0\cos\alpha\right),\quad(43)$$

$$W_4'\left(l_0\cos\alpha\right)=e^{i\kappa 2l_0\cos\alpha}W_3'\left(-l_0\cos\alpha\right),\ M_4\left(l_0\cos\alpha\right)=e^{i\kappa 2l_0\cos\alpha}M_3\left(-l_0\cos\alpha\right),$$

$$N_4\left(l_0\cos\alpha\right)+\cos\alpha N_6\left(l_0\right)=e^{i\kappa 2l_0\cos\alpha}\left[N_3\left(-l_0\cos\alpha\right)+\cos\alpha N_5\left(-l_0\right)\right],$$

$$Q_4\left(l_0\cos\alpha\right)+\sin\alpha N_6\left(l_0\right)=e^{i\kappa 2l_0\cos\alpha}\left[Q_3\left(-l_0\cos\alpha\right)-\sin\alpha N_5\left(-l_0\right)\right].$$

Eqs. (42) and (43) give a group of algebraic equations, which can be expressed as:

$$\mathbf{TX}=0,\tag{44}$$

in which $\mathbf{X}$ is a column vector expressed as:

$$\mathbf{X}=\{A_1\quad B_1\quad A_2\quad B_2\quad C_1\quad D_1\quad E_1\quad F_1\quad C_2\quad D_2\quad E_2\quad F_2\quad A_3\quad B_3\quad A_4\quad B_4$$
$$C_3\quad D_3\quad E_3\quad F_3\quad C_4\quad D_4\quad E_4\quad F_4\quad A_5\quad B_5\quad A_6\quad B_6\}^{\mathrm{T}},$$

and the elements of Matrix $\mathbf{T}$ are presented in the Appendix.

The dispersion relations for the corrugated sandwich plate can be obtained by solving the following equation:

$$\det\left(\mathbf{T}\right)=0.\tag{45}$$

3. Results and discussions

In order to validate the developed dynamic homogenization model, the dispersion relations obtained from the homogenization method are compared with those obtained from the spectral element method. For the special case that the thickness of the core sheets approaches to zero, the sandwich plate degenerates to two independent homogeneous face sheets. Such a simple case is firstly considered. For a homogeneous plate, both the dispersion relations of bending wave and longitudinal wave have exact solutions [40]:

$$\omega_b=\kappa_b^2\sqrt{D/\left(\rho t\right)},\ \omega_l=\kappa_l\sqrt{A/\left(\rho t\right)}\tag{46}$$

where the subscripts b and l represent the bending wave and longitudinal wave, ρ is the mass density of the homogeneous material, t is the thickness, $D=Et^3/\left[12\left(1-v^2\right)\right]$ and $A=Et/\left(1-v^2\right)$ are respectively the bending stiffness and stretching stiffness of the plate, in which E and v are the Young's modulus and Poisson's ratio. The dispersion curves predicted by the developed dynamic

14

homogenization model, the spectral element method, and Eq. (46) are compared in Fig.2. The dimensionless frequency and dimensionless wavenumber are respectively defined as $\bar{\omega} = \omega a/c$ and $\bar{\kappa} = \kappa a$, where $c = \sqrt{A/(\rho t)}$ is the velocity of in-plane longitudinal wave in homogeneous isotropic thin plates. Fig.2 shows that both the dynamic homogenization method and the spectral element method give the same results with the exact solutions.

Then, a corrugated sandwich plate with the following material and geometric parameters is considered:

$$E_f = 70 \text{ GPa}, \quad \rho_f = 2700 \text{ kg/m}^3, \quad \nu_f = 0.3, \quad t_f = 0.002 \text{ m}, \quad E_c = 2.4 \text{ GPa},$$

$$\rho_c = 1040 \text{ kg/m}^3, \quad \nu_c = 0.38, \quad t_c = 0.001 \text{ m}, \quad l_0 = 0.015 \text{ m}.$$

The dispersion curves obtained by the homogenization method and the spectral element method are compared in Fig.3, in which the dimensionless frequency is defined as $\bar{\omega} = \omega a/c_f$ with $c_f = \sqrt{A_f/(\rho_f t_f)}$ and $a = 2l_0 \cos\alpha$. Fig.3 shows that for waves with relatively low frequencies, the dispersion curves obtained by the homogenization method agree well with those obtained by the spectral element method. For the two branches with lowest frequencies, the developed homogenization model gives almost the same results with the spectral element method even in the full wavenumber range.

The dispersion curves for corrugated sandwich plates based on the developed homogenization model can be seen more clearly in Fig.4. It displays that the present dynamic homogenization method can predict four branches of dispersion curves, as well as the corresponding wave modes. 'BE', 'L', 'BR' and 'S' labeled in Fig.4(a) denote the bending wave mode, longitudinal wave mode, breathing mode, and shear wave mode, respectively. These wave modes are depicted in Fig.5. The corrugated sandwich plate can also be treated as an equivalent homogeneous Mindlin plate by calculating the effective shear modulus of the corrugated core with a simple method adopted in Refs. [41, 42]. The dispersion curves predicted by this simple equivalent model are also displayed in Fig.4. It shows that the simple equivalent model gives only two branches of the dispersion curves (respectively corresponding to the bending and shear wave modes). Moreover, via comparing with the numerical solutions obtained by finite element software COMSOL, it is evident that for both the cases of the inclination angle $\alpha = \pi/4$ and $\alpha = \pi/6$, the simple equivalent model provides

15

acceptable dispersion curve of the bending wave only when the wavenumber is comparatively small, and with the increase of the wavenumber, the relative error of the results predicted by the simple equivalent model increases significantly. In contrast, the dispersion relations for both the bending wave mode and breathing mode predicted by the present homogenization model show good accuracy in almost the whole wavenumber range. This is mainly because the microstructural periodicity, which is neglected in the simple equivalent method, is accurately captured in the present homogenization model via introducing the shifting operator.

The effects of some geometric and material parameters on the dispersion relations for the corrugated sandwich plate are also discussed. We focus only on the lowest two branches of the dispersion curves. The following parameters are kept constant in the analyses:

$$E_f = 70 \text{ GPa}, \quad \rho_f = 2700 \text{ kg}/\text{m}^3, \quad \nu_f = \nu_c = 0.3, \text{ and } h_c = 0.01 \text{ m},$$

where h_c denotes the height of the core layer, and $h_c = l_0 \sin \alpha$.

Firstly, the effect of the thickness t_c of the core sheets on the dispersion relations is investigated. As shown in Fig.6, with the increase of t_c, the group velocity (corresponding to a specified wavenumber) of the longitudinal wave decreases slightly, while that of the bending wave increases. Moreover, the dispersion curve corresponding to the breathing mode moves upwards. These phenomena can be explained as follows. The dispersion relation of the longitudinal wave can be approximately expressed as:

$$\omega_l = \kappa_l \sqrt{2E_f t_f \Big/ \left[\left(1-\nu_f^2\right)\left(2\rho_f t_f + \rho_c t_c / \cos \alpha\right)\right]}, \tag{47}$$

which shows that the tangent slope of the corresponding dispersion curve decreases slightly with the increase of t_c. Moreover, the shear stiffness and the out-of-plane compressive (or tensile) stiffness of the sandwich plate are mainly contributed by the core, and they are both enhanced as the thickness of the core sheets increases. With the increase of the shear stiffness, the group velocity of the bending wave increases; and with the increase of the out-of-plane compressive stiffness, the dispersion curve corresponding to the breathing mode moves upwards.

Then, the effect of the inclination angle of the core sheets on the dispersion relations is displayed in Fig.7. It should be noted that the frequency and wavenumber

16

in this figure are nondimensionalized by using h_c instead of a, which is different from those in other figures, since under the condition that h_c is kept constant, the length of each unit cell a varies with the inclination angle α. Fig.7 shows that with the increase of the inclination angle, the dispersion curves of the longitudinal and bending waves vary slightly, while that corresponding to the breathing mode moves upwards evidently. This is mainly attributed to the increase of the out-of-plane compressive stiffness of the sandwich plate caused by the increase of the inclination angle.

Fig.8 shows the effect of the thickness t_f of the face sheets on the dispersion relations. It displays that the group velocity of the longitudinal wave increases slightly with t_f. This result can also be predicted by Eq. (47). Fig.8 also shows that with the increase of t_f, the group velocity of the bending wave decreases. Actually, both the bending stiffness and the mass density of the sandwich plate increase with the increase of the thickness of the face sheets. The group velocity of the bending wave increases as the bending stiffness increases, but decreases as the mass density increases. Since the mass density plays a relatively more important role, the group velocity of the bending wave decreases. Moreover, the dispersion curve corresponding to the breathing mode moves downwards with the increase of t_f.

The effect of the Young's modulus E_c of the corrugated core on the dispersion relations is displayed in Fig.9, which shows that with the increase of E_c, the group velocity of the longitudinal wave nearly keeps constant, while the group velocity of the bending wave increases. The former phenomenon can be predicted by Eq. (47), which demonstrates that the group velocity of the longitudinal wave is independent of E_c, and the latter one is due to the fact that the shear stiffness of the sandwich plate increases with the increase of E_c, so does the group velocity of the bending wave. Moreover, owing to the increase of the out-of-plane compressive stiffness of the sandwich plate caused by the increase of E_c, the dispersion curve corresponding to the breathing mode moves upwards.

Furthermore, the effect of the density ρ_c of the corrugated core on the dispersion relations for the sandwich plate is studied and shown in Fig.10. It displays that the dispersion curves corresponding to all the three considered wave modes move

downwards, This is due to the fact that the mass density increases with ρ_c.

4. Conclusions

A dynamic homogenization model is developed in the present work to investigate the long-wavelength wave propagation in corrugated sandwich plates. Via defining a shifting operator and adopting the harmonic motion assumption, the equations of motion are firstly represented in a state-space form. Then by employing a two-scale homogenization method to derive a homogenization model and considering sinusoidal wave propagation, an eigenvalue problem is obtained, from which the dispersion relations and corresponding wave modes can be determined. Benchmark solutions for the dispersion relations are also provided by using the spectral element method. Numerical results demonstrate that the developed dynamic homogenization model gives good results for four branches of dispersion curves (corresponding to bending wave mode, longitudinal wave mode, breathing mode, and shear wave mode, respectively) in the low-frequency range. Parameter studies are also carried out to investigate the effects of geometric and material parameters on the dispersion relations of the sandwich plate. It should be pointed out that the developed homogenization model can be further used to analyze other mechanical properties of corrugated sandwich plates, and the present homogenization method is also applicable to three-dimensional sandwich structures with various lattice truss cores, such as pyramidal and tetrahedral lattices.

Appendix

Elements of Matrix $\mathbf{B}^{\varepsilon}$

$$B_{1,2}^{\varepsilon} = 1,$$

$$B_{2,1}^{\varepsilon} = -\omega^2 \left\{ \rho_f t_f + \rho_c t_c l_0 \sum_{n=1}^{\infty} \delta\left[x - 2(n-1)l_0 \cos\alpha\right] \right\} + \left(2A_c \cos^2\alpha/l_0\right) \sum_{n=1}^{\infty} \delta\left[x - 2(n-1)l_0 \cos\alpha\right],$$

$$B_{2,7}^{\varepsilon} = -\left(A_c \cos^2\alpha/l_0\right) \sum_{n=1}^{\infty} \delta\left[x - 2(n-1)l_0 \cos\alpha\right]\left(\Delta_{l_0 \cos\alpha} + \Delta_{-l_0 \cos\alpha}\right),$$

$$B_{2,9}^{\varepsilon} = -\left(A_c \sin\alpha\cos\alpha/l_0\right) \sum_{n=1}^{\infty} \delta\left[x - 2(n-1)l_0 \cos\alpha\right]\left(\Delta_{l_0 \cos\alpha} - \Delta_{-l_0 \cos\alpha}\right),$$

$$B_{3,4}^{\varepsilon} = 1, \quad B_{4,5}^{\varepsilon} = 1, \quad B_{5,6}^{\varepsilon} = 1,$$

$$B_{6,3}^{\varepsilon} = \omega^2 \left\{ \rho_f t_f + \rho_c t_c l_0 \sum_{n=1}^{\infty} \delta\left[x - 2(n-1)l_0 \cos\alpha\right] \right\} - \left(2A_c \sin^2\alpha/l_0\right) \sum_{n=1}^{\infty} \delta\left[x - 2(n-1)l_0 \cos\alpha\right],$$

$$B_{6,7}^{\varepsilon} = \left(A_c \sin\alpha\cos\alpha/l_0\right) \sum_{n=1}^{\infty} \delta\left[x - 2(n-1)l_0 \cos\alpha\right]\left(\Delta_{l_0 \cos\alpha} - \Delta_{-l_0 \cos\alpha}\right),$$

$$B_{6,9}^{\varepsilon} = \left(A_c \sin^2\alpha/l_0\right) \sum_{n=1}^{\infty} \delta\left[x - 2(n-1)l_0 \cos\alpha\right]\left(\Delta_{l_0 \cos\alpha} + \Delta_{-l_0 \cos\alpha}\right), \quad B_{7,8}^{\varepsilon} = 1,$$

$$B_{8,1}^{\varepsilon} = -\left(A_c \cos^2\alpha/l_0\right) \sum_{n=1}^{\infty} \left\{ \delta\left[x - (2n-3)l_0 \cos\alpha\right]\Delta_{-l_0 \cos\alpha} + \delta\left[x - (2n-1)l_0 \cos\alpha\right]\Delta_{l_0 \cos\alpha} \right\},$$

$$B_{8,3}^{\varepsilon} = -\left(A_c \sin\alpha\cos\alpha/l_0\right) \sum_{n=1}^{\infty} \left\{ \delta\left[x - (2n-3)l_0 \cos\alpha\right]\Delta_{-l_0 \cos\alpha} - \delta\left[x - (2n-1)l_0 \cos\alpha\right]\Delta_{l_0 \cos\alpha} \right\},$$

$$B_{8,7}^{\varepsilon} = -\omega^2 \left\{ \rho_f t_f + \left(\rho_c t_c l_0/2\right) \sum_{n=1}^{\infty} \delta\left[x - (2n-3)l_0 \cos\alpha\right] + \left(\rho_c t_c l_0/2\right) \sum_{n=1}^{\infty} \delta\left[x - (2n-1)l_0 \cos\alpha\right] \right\}$$
$$+ \left(A_c \cos^2\alpha/l_0\right) \sum_{n=1}^{\infty} \left\{ \delta\left[x - (2n-3)l_0 \cos\alpha\right] + \delta\left[x - (2n-1)l_0 \cos\alpha\right] \right\},$$

$$B_{8,9}^{\varepsilon} = \left(A_c \sin\alpha\cos\alpha/l_0\right) \sum_{n=1}^{\infty} \left\{ \delta\left[x - (2n-3)l_0 \cos\alpha\right] - \delta\left[x - (2n-1)l_0 \cos\alpha\right] \right\}, \quad B_{9,10}^{\varepsilon} = 1,$$

$$B_{10,11}^{\varepsilon} = 1, \quad B_{11,12}^{\varepsilon} = 1,$$

$$B_{12,1}^{\varepsilon} = \left(A_c \sin\alpha\cos\alpha/l_0\right) \sum_{n=1}^{\infty} \left\{ \delta\left[x - (2n-3)l_0 \cos\alpha\right]\Delta_{-l_0 \cos\alpha} - \delta\left[x - (2n-1)l_0 \cos\alpha\right]\Delta_{l_0 \cos\alpha} \right\},$$

$$B_{12,3}^{\varepsilon} = \left(A_c \sin^2\alpha/l_0\right) \sum_{n=1}^{\infty} \left\{ \delta\left[x - (2n-3)l_0 \cos\alpha\right]\Delta_{-l_0 \cos\alpha} + \delta\left[x - (2n-1)l_0 \cos\alpha\right]\Delta_{l_0 \cos\alpha} \right\},$$

$$B_{12,7}^{\varepsilon} = -\left(A_c \sin\alpha\cos\alpha/l_0\right) \sum_{n=1}^{\infty} \left\{ \delta\left[x - (2n-3)l_0 \cos\alpha\right] - \delta\left[x - (2n-1)l_0 \cos\alpha\right] \right\},$$

19

$$B_{12,9}^{\varepsilon} = \omega^2 \left\{ \rho_f t_f + \left(\rho_c t_c l_0/2 \right) \sum_{n=1}^{\infty} \delta \left[x - (2n-3) l_0 \cos\alpha \right] + \left(\rho_c t_c l_0/2 \right) \sum_{n=1}^{\infty} \delta \left[x - (2n-1) l_0 \cos\alpha \right] \right\}$$

$$- \left(A_c \sin^2\alpha / l_0 \right) \sum_{n=1}^{\infty} \left\{ \delta \left[x - (2n-3) l_0 \cos\alpha \right] + \delta \left[x - (2n-1) l_0 \cos\alpha \right] \right\},$$

all the other elements of Matrix $\mathbf{B}^{\varepsilon}$ are equal to zero.

Elements of Matrix $\bar{\mathbf{C}}_{\text{hom}}$

$$\bar{C}_{\text{hom}1,2} = 1/A_f , \quad \bar{C}_{\text{hom}2,1} = -\omega^2 \left[\rho_f t_f + \rho_c t_c / (2\cos\alpha) \right] + A_c \cos\alpha / l_0^2 ,$$

$$\bar{C}_{\text{hom}2,7} = -\left(A_c \cos\alpha / l_0^2 \right) \cos\left(\kappa l_0 \cos\alpha \right), \quad \bar{C}_{\text{hom}2,9} = \left(i A_c \sin\alpha / l_0^2 \right) \sin\left(\kappa l_0 \cos\alpha \right), \quad \bar{C}_{\text{hom}3,4} = 1,$$

$$\bar{C}_{\text{hom}4,5} = 1/D_f , \quad \bar{C}_{\text{hom}5,6} = 1, \quad \bar{C}_{\text{hom}6,3} = \omega^2 \left[\rho_f t_f + \rho_c t_c / (2\cos\alpha) \right] - A_c \sin^2\alpha / \left(l_0^2 \cos\alpha \right),$$

$$\bar{C}_{\text{hom}6,7} = -\left(i A_c \sin\alpha / l_0^2 \right) \sin\left(\kappa l_0 \cos\alpha \right), \quad \bar{C}_{\text{hom}6,9} = \left[A_c \sin^2\alpha / \left(l_0^2 \cos\alpha \right) \right] \cos\left(\kappa l_0 \cos\alpha \right),$$

$$\bar{C}_{\text{hom}7,8} = 1/A_f , \quad \bar{C}_{\text{hom}8,1} = -\left(A_c \cos\alpha / l_0^2 \right) \cos\left(\kappa l_0 \cos\alpha \right),$$

$$\bar{C}_{\text{hom}8,3} = -\left(i A_c \sin\alpha / l_0^2 \right) \sin\left(\kappa l_0 \cos\alpha \right), \quad \bar{C}_{\text{hom}8,7} = -\omega^2 \left[\rho_f t_f + \rho_c t_c / (2\cos\alpha) \right] + A_c \cos\alpha / l_0^2 ,$$

$$\bar{C}_{\text{hom}9,10} = 1, \quad \bar{C}_{\text{hom}10,11} = 1/D_f , \quad \bar{C}_{\text{hom}11,12} = 1, \quad \bar{C}_{\text{hom}12,1} = \left(i A_c \sin\alpha / l_0^2 \right) \sin\left(\kappa l_0 \cos\alpha \right),$$

$$\bar{C}_{\text{hom}12,3} = \left[A_c \sin^2\alpha / \left(l_0^2 \cos\alpha \right) \right] \cos\left(\kappa l_0 \cos\alpha \right),$$

$$\bar{C}_{\text{hom}12,9} = \omega^2 \left[\rho_f t_f + \rho_c t_c / (2\cos\alpha) \right] - A_c \sin^2\alpha / \left(l_0^2 \cos\alpha \right),$$

all the other elements of Matrix $\bar{\mathbf{C}}_{\text{hom}}$ are equal to zero.

Expressions for $c_i \left(i = 1, 2, \cdots, 5 \right)$ **and** Δ

$$c_1 = m^4, \quad c_2 = -2 \left[A_c \sec\alpha + \kappa^2 l_0^2 \left(A_f + \kappa^2 D_f \right) \right] m^3 / l_0^2 ,$$

$$c_3 = \left\{ A_c^2 \left\{ \tan^2\alpha \left[1 + 3\cos(2\alpha) \cos(2\kappa l_0 \cos\alpha) \right] + 2\tan^2\alpha \cos^2\left(\kappa l_0 \cos\alpha \right) \right. \right.$$
$$\left. + 4\cos^2\alpha \sin^2\left(\kappa l_0 \cos\alpha \right) + 10\sin^2\alpha \right\} + 8 A_c \kappa^2 l_0^2 \left[\left(A_f + 2\kappa^2 D_f \right) \cos\alpha \right.$$
$$\left. \left. + \left(2A_f + \kappa^2 D_f \right) \sin\alpha \tan\alpha \right] + 4\kappa^4 l_0^4 \left(A_f^2 + 4\kappa^2 A_f D_f + \kappa^4 D_f^2 \right) \right\} m^2 / \left(4 l_0^4 \right),$$

$$c_4 = -\kappa^2 \left\{ \left[3A_c^2 - A_c^2 \cos(4\alpha) + 8\kappa^6 l_0^4 A_f D_f \cos^2\alpha \right] \left(A_f + \kappa^2 D_f \right) \right.$$
$$+ 2 A_c \kappa^2 l_0^2 \left[\left(A_f^2 + 8\kappa^2 A_f D_f + 3\kappa^4 D_f^2 \right) \cos\alpha - \left(A_f^2 - \kappa^4 D_f^2 \right) \cos(3\alpha) \right]$$
$$- 2 A_c^2 \left(A_f - \kappa^2 D_f \right) \cos(2\alpha)$$
$$\left. + 4 A_c^2 \left(A_f \sin^2\alpha - \kappa^2 D_f \cos^2\alpha \right) \cos(2\alpha) \cos(2\kappa l_0 \cos\alpha) \right\} \sec^2\alpha \, m / \left(4 l_0^4 \right),$$

$$c_5 = \kappa^4 \left\{ A_c^2 \left[3\left(A_f^2 + 2\kappa^2 A_f D_f + \kappa^4 D_f^2 \right) - 4\left(A_f^2 - \kappa^4 D_f^2 \right)\cos(2\alpha) \right. \right.$$
$$\left. + \left(A_f^2 - 6\kappa^2 A_f D_f + \kappa^4 D_f^2 \right)\cos(4\alpha) \right] + 16\kappa^8 l_0^4 A_f^2 D_f^2 \cos^2\alpha$$
$$+ 8\kappa^4 l_0^2 A_c A_f D_f \left\{ A_f \left[\cos\alpha - \cos(3\alpha) \right] + \kappa^2 D_f \left[3\cos\alpha + \cos(3\alpha) \right] \right\}$$
$$\left. - 2A_c^2 \left[A_f - \kappa^2 D_f - \left(A_f + \kappa^2 D_f \right)\cos(2\alpha) \right]^2 \cos(2\kappa l_0 \cos\alpha) \right\} \sec^2\alpha / \left(16 l_0^4 \right),$$

where $m = \rho_f t_f + \rho_c t_c / (2\cos\alpha)$.

Moreover, $\Delta = \dfrac{\sqrt[3]{2}\Delta_1}{3c_1\sqrt[3]{\Delta_2 + \sqrt{-4\Delta_1^3 + \Delta_2^2}}} + \dfrac{\sqrt[3]{\Delta_2 + \sqrt{-4\Delta_1^3 + \Delta_2^2}}}{3\sqrt[3]{2}c_1}$,

where $\Delta_1 = c_3^2 - 3c_2 c_4 + 12 c_1 c_5$, and $\Delta_2 = 2c_3^3 - 9c_2 c_3 c_4 + 27 c_1 c_4^2 + 27 c_2^2 c_5 - 72 c_1 c_3 c_5$.

Specifically, for the case that the inclination angle of the core sheets $\alpha = \pi/4$, the coefficients $c_i \left(i = 1, 2, \cdots, 5 \right)$ read:

$$c_1 = m^4, \quad c_2 = -2\left[\sqrt{2}A_c + \kappa^2 l_0^2 \left(A_f + \kappa^2 D_f \right) \right] m^3 / l_0^2,$$

$$c_3 = \left[2A_c^2 + 3\sqrt{2}A_c \kappa^2 l_0^2 \left(A_f + \kappa^2 D_f \right) + \kappa^4 l_0^4 \left(A_f^2 + 4\kappa^2 A_f D_f + \kappa^4 D_f^2 \right) \right] m^2 / l_0^4,$$

$$c_4 = -\kappa^2 \left[2\left(A_c^2 + \kappa^6 l_0^4 A_f D_f \right)\left(A_f + \kappa^2 D_f \right) + \sqrt{2}A_c \kappa^2 l_0^2 \left(A_f^2 + 4\kappa^2 A_f D_f + \kappa^4 D_f^2 \right) \right] m / l_0^4,$$

$$c_5 = \kappa^4 \left[A_c^2 \left(A_f^2 + 6\kappa^2 A_f D_f + \kappa^4 D_f^2 \right) + 4\sqrt{2}\kappa^4 l_0^2 A_c A_f D_f \left(A_f + \kappa^2 D_f \right) + 4\kappa^8 l_0^4 A_f^2 D_f^2 \right.$$
$$\left. - A_c^2 \left(A_f - \kappa^2 D_f \right)^2 \cos\left(\sqrt{2}\kappa l_0 \right) \right] / 4l_0^4.$$

Elements of Matrix T

$T_{1,2} = 1, \quad T_{1,4} = -1, \quad T_{2,6} = 1, \quad T_{2,8} = 1, \quad T_{2,10} = -1, \quad T_{2,12} = -1, \quad T_{3,5} = 1, \quad T_{3,7} = 1,$

$T_{3,9} = -1, \quad T_{3,11} = -1, \quad T_{4,1} = A_f k_f, \quad T_{4,3} = -A_f k_f, \quad T_{4,25} = \cos\alpha A_c k_c,$

$T_{4,27} = -\cos\alpha A_c k_c, \quad T_{5,5} = D_f \lambda^3, \quad T_{5,7} = -D_f \lambda^3, \quad T_{5,9} = -D_f \lambda^3, \quad T_{5,11} = D_f \lambda^3,$

$T_{5,25} = -\sin\alpha A_c k_c, \quad T_{5,27} = -\sin\alpha A_c k_c, \quad T_{6,6} = 1, \quad T_{6,8} = -1, \quad T_{6,10} = -1, \quad T_{6,12} = 1,$

$T_{7,14} = 1, \quad T_{7,16} = -1, \quad T_{8,18} = 1, \quad T_{8,20} = 1, \quad T_{8,22} = -1, \quad T_{8,24} = -1, \quad T_{9,17} = 1, \quad T_{9,19} = 1,$

$T_{9,21} = -1, \quad T_{9,23} = -1, \quad T_{10,13} = 1, \quad T_{10,15} = -1, \quad T_{11,17} = 1, \quad T_{11,19} = -1, \quad T_{11,21} = -1,$

$T_{11,23} = 1, \quad T_{12,18} = 1, \quad T_{12,20} = -1, \quad T_{12,22} = -1, \quad T_{12,24} = 1, \quad T_{13,2} = \cos\alpha, \quad T_{13,6} = \sin\alpha,$

$T_{13,8} = \sin\alpha, \quad T_{13,26} = -1, \quad T_{14,2} = \cos\alpha, \quad T_{14,6} = -\sin\alpha, \quad T_{14,8} = -\sin\alpha, \quad T_{14,28} = -1,$

21

$$T_{15,13} = -\cos\alpha\sin\left(k_f l_0 \cos\alpha\right), \quad T_{15,14} = \cos\alpha\cos\left(k_f l_0 \cos\alpha\right),$$

$$T_{15,17} = -\sin\alpha\sinh\left(\lambda l_0 \cos\alpha\right), \quad T_{15,18} = \sin\alpha\cosh\left(\lambda l_0 \cos\alpha\right),$$

$$T_{15,19} = -\sin\alpha\sin\left(\lambda l_0 \cos\alpha\right), \quad T_{15,20} = \sin\alpha\cos\left(\lambda l_0 \cos\alpha\right), \quad T_{15,25} = \sin\left(k_c l_0\right),$$

$$T_{15,26} = -\cos\left(k_c l_0\right), \quad T_{16,15} = \cos\alpha\sin\left(k_f l_0 \cos\alpha\right), \quad T_{16,16} = \cos\alpha\cos\left(k_f l_0 \cos\alpha\right),$$

$$T_{16,21} = -\sin\alpha\sinh\left(\lambda l_0 \cos\alpha\right), \quad T_{16,22} = -\sin\alpha\cosh\left(\lambda l_0 \cos\alpha\right),$$

$$T_{16,23} = -\sin\alpha\sin\left(\lambda l_0 \cos\alpha\right), \quad T_{16,24} = -\sin\alpha\cos\left(\lambda l_0 \cos\alpha\right), \quad T_{16,27} = -\sin\left(k_c l_0\right),$$

$$T_{16,28} = -\cos\left(k_c l_0\right), \quad T_{17,1} = -e^{i\kappa 2l_0 \cos\alpha}\sin\left(k_f l_0 \cos\alpha\right), \quad T_{17,2} = e^{i\kappa 2l_0 \cos\alpha}\cos\left(k_f l_0 \cos\alpha\right),$$

$$T_{17,3} = -\sin\left(k_f l_0 \cos\alpha\right), \quad T_{17,4} = -\cos\left(k_f l_0 \cos\alpha\right), \quad T_{18,5} = -e^{i\kappa 2l_0 \cos\alpha}\sinh\left(\lambda l_0 \cos\alpha\right),$$

$$T_{18,6} = e^{i\kappa 2l_0 \cos\alpha}\cosh\left(\lambda l_0 \cos\alpha\right), \quad T_{18,7} = -e^{i\kappa 2l_0 \cos\alpha}\sin\left(\lambda l_0 \cos\alpha\right), \quad T_{18,8} = e^{i\kappa 2l_0 \cos\alpha}\cos\left(\lambda l_0 \cos\alpha\right),$$

$$T_{18,9} = -\sinh\left(\lambda l_0 \cos\alpha\right), \quad T_{18,10} = -\cosh\left(\lambda l_0 \cos\alpha\right), \quad T_{18,11} = -\sin\left(\lambda l_0 \cos\alpha\right),$$

$$T_{18,12} = -\cos\left(\lambda l_0 \cos\alpha\right), \quad T_{19,5} = e^{i\kappa 2l_0 \cos\alpha}\cosh\left(\lambda l_0 \cos\alpha\right), \quad T_{19,6} = -e^{i\kappa 2l_0 \cos\alpha}\sinh\left(\lambda l_0 \cos\alpha\right),$$

$$T_{19,7} = e^{i\kappa 2l_0 \cos\alpha}\cos\left(\lambda l_0 \cos\alpha\right), \quad T_{19,8} = e^{i\kappa 2l_0 \cos\alpha}\sin\left(\lambda l_0 \cos\alpha\right), \quad T_{19,9} = -\cosh\left(\lambda l_0 \cos\alpha\right),$$

$$T_{19,10} = -\sinh\left(\lambda l_0 \cos\alpha\right), \quad T_{19,11} = -\cos\left(\lambda l_0 \cos\alpha\right), \quad T_{19,12} = \sin\left(\lambda l_0 \cos\alpha\right),$$

$$T_{20,1} = e^{i\kappa 2l_0 \cos\alpha}\cos\left(k_f l_0 \cos\alpha\right), \quad T_{20,2} = e^{i\kappa 2l_0 \cos\alpha}\sin\left(k_f l_0 \cos\alpha\right), \quad T_{20,3} = -\cos\left(k_f l_0 \cos\alpha\right),$$

$$T_{20,4} = \sin\left(k_f l_0 \cos\alpha\right), \quad T_{21,5} = e^{i\kappa 2l_0 \cos\alpha}\cosh\left(\lambda l_0 \cos\alpha\right), \quad T_{21,6} = -e^{i\kappa 2l_0 \cos\alpha}\sinh\left(\lambda l_0 \cos\alpha\right),$$

$$T_{21,7} = -e^{i\kappa 2l_0 \cos\alpha}\cos\left(\lambda l_0 \cos\alpha\right), \quad T_{21,8} = -e^{i\kappa 2l_0 \cos\alpha}\sin\left(\lambda l_0 \cos\alpha\right), \quad T_{21,9} = -\cosh\left(\lambda l_0 \cos\alpha\right),$$

$$T_{21,10} = -\sinh\left(\lambda l_0 \cos\alpha\right), \quad T_{21,11} = \cos\left(\lambda l_0 \cos\alpha\right), \quad T_{21,12} = -\sin\left(\lambda l_0 \cos\alpha\right),$$

$$T_{22,5} = -e^{i\kappa 2l_0 \cos\alpha}\sinh\left(\lambda l_0 \cos\alpha\right), \quad T_{22,6} = e^{i\kappa 2l_0 \cos\alpha}\cosh\left(\lambda l_0 \cos\alpha\right),$$

$$T_{22,7} = e^{i\kappa 2l_0 \cos\alpha}\sin\left(\lambda l_0 \cos\alpha\right), \quad T_{22,8} = -e^{i\kappa 2l_0 \cos\alpha}\cos\left(\lambda l_0 \cos\alpha\right), \quad T_{22,9} = -\sinh\left(\lambda l_0 \cos\alpha\right),$$

$$T_{22,10} = -\cosh\left(\lambda l_0 \cos\alpha\right), \quad T_{22,11} = \sin\left(\lambda l_0 \cos\alpha\right), \quad T_{22,12} = \cos\left(\lambda l_0 \cos\alpha\right),$$

$$T_{23,13} = -e^{i\kappa 2l_0 \cos\alpha}\sin\left(k_f l_0 \cos\alpha\right), \quad T_{23,14} = e^{i\kappa 2l_0 \cos\alpha}\cos\left(k_f l_0 \cos\alpha\right), \quad T_{23,15} = -\sin\left(k_f l_0 \cos\alpha\right),$$

$$T_{23,16} = -\cos\left(k_f l_0 \cos\alpha\right), \quad T_{24,17} = -e^{i\kappa 2l_0 \cos\alpha}\sinh\left(\lambda l_0 \cos\alpha\right), \quad T_{24,18} = e^{i\kappa 2l_0 \cos\alpha}\cosh\left(\lambda l_0 \cos\alpha\right),$$

22

$T_{24,19} = -e^{i\kappa 2l_0 \cos\alpha} \sin(\lambda l_0 \cos\alpha), \quad T_{24,20} = e^{i\kappa 2l_0 \cos\alpha} \cos(\lambda l_0 \cos\alpha), \quad T_{24,21} = -\sinh(\lambda l_0 \cos\alpha),$

$T_{24,22} = -\cosh(\lambda l_0 \cos\alpha), \quad T_{24,23} = -\sin(\lambda l_0 \cos\alpha), \quad T_{24,24} = -\cos(\lambda l_0 \cos\alpha),$

$T_{25,17} = e^{i\kappa 2l_0 \cos\alpha} \cosh(\lambda l_0 \cos\alpha), \quad T_{25,18} = -e^{i\kappa 2l_0 \cos\alpha} \sinh(\lambda l_0 \cos\alpha),$

$T_{25,19} = e^{i\kappa 2l_0 \cos\alpha} \cos(\lambda l_0 \cos\alpha), \quad T_{25,20} = e^{i\kappa 2l_0 \cos\alpha} \sin(\lambda l_0 \cos\alpha), \quad T_{25,21} = -\cosh(\lambda l_0 \cos\alpha),$

$T_{25,22} = -\sinh(\lambda l_0 \cos\alpha), \quad T_{25,23} = -\cos(\lambda l_0 \cos\alpha), \quad T_{25,24} = \sin(\lambda l_0 \cos\alpha),$

$T_{26,13} = e^{i\kappa 2l_0 \cos\alpha} A_f k_f \cos(k_f l_0 \cos\alpha), \quad T_{26,14} = e^{i\kappa 2l_0 \cos\alpha} A_f k_f \sin(k_f l_0 \cos\alpha),$

$T_{26,15} = -A_f k_f \cos(k_f l_0 \cos\alpha), \quad T_{26,16} = A_f k_f \sin(k_f l_0 \cos\alpha),$

$T_{26,25} = e^{i\kappa 2l_0 \cos\alpha} \cos\alpha A_c k_c \cos(k_c l_0), \quad T_{26,26} = e^{i\kappa 2l_0 \cos\alpha} \cos\alpha A_c k_c \sin(k_c l_0),$

$T_{26,27} = -\cos\alpha A_c k_c \cos(k_c l_0), \quad T_{26,28} = \cos\alpha A_c k_c \sin(k_c l_0),$

$T_{27,17} = e^{i\kappa 2l_0 \cos\alpha} D_f \lambda^3 \cosh(\lambda l_0 \cos\alpha), \quad T_{27,18} = -e^{i\kappa 2l_0 \cos\alpha} D_f \lambda^3 \sinh(\lambda l_0 \cos\alpha),$

$T_{27,19} = -e^{i\kappa 2l_0 \cos\alpha} D_f \lambda^3 \cos(\lambda l_0 \cos\alpha), \quad T_{27,20} = -e^{i\kappa 2l_0 \cos\alpha} D_f \lambda^3 \sin(\lambda l_0 \cos\alpha),$

$T_{27,21} = -D_f \lambda^3 \cosh(\lambda l_0 \cos\alpha), \quad T_{27,22} = -D_f \lambda^3 \sinh(\lambda l_0 \cos\alpha),$

$T_{27,23} = D_f \lambda^3 \cos(\lambda l_0 \cos\alpha), \quad T_{27,24} = -D_f \lambda^3 \sin(\lambda l_0 \cos\alpha),$

$T_{27,25} = -e^{i\kappa 2l_0 \cos\alpha} \sin\alpha A_c k_c \cos(k_c l_0), \quad T_{27,26} = -e^{i\kappa 2l_0 \cos\alpha} \sin\alpha A_c k_c \sin(k_c l_0),$

$T_{27,27} = -\sin\alpha A_c k_c \cos(k_c l_0), \quad T_{27,28} = \sin\alpha A_c k_c \sin(k_c l_0),$

$T_{28,17} = -e^{i\kappa 2l_0 \cos\alpha} \sinh(\lambda l_0 \cos\alpha), \quad T_{28,18} = e^{i\kappa 2l_0 \cos\alpha} \cosh(\lambda l_0 \cos\alpha),$

$T_{28,19} = e^{i\kappa 2l_0 \cos\alpha} \sin(\lambda l_0 \cos\alpha), \quad T_{28,20} = -e^{i\kappa 2l_0 \cos\alpha} \cos(\lambda l_0 \cos\alpha), \quad T_{28,21} = -\sinh(\lambda l_0 \cos\alpha),$

$T_{28,22} = -\cosh(\lambda l_0 \cos\alpha), \quad T_{28,23} = \sin(\lambda l_0 \cos\alpha), \quad T_{28,24} = \cos(\lambda l_0 \cos\alpha),$

all the other elements of Matrix $\mathbf{T}$ are equal to zero.

References

[1] Wang B, Wu L, Ma L, Sun Y, Du S. Mechanical behavior of the sandwich structures with carbon fiber-reinforced pyramidal lattice truss core. Materials & Design. 2010;31:2659-63.

[2] Wang B, Wu LZ, Ma L, Feng JC. Low-velocity impact characteristics and residual tensile strength of carbon fiber composite lattice core sandwich structures. Composites part B: engineering. 2011;42:891-7.

[3] Wang B, Wu L, Jin X, Du S, Sun Y, Ma L. Experimental investigation of 3D sandwich structure with core reinforced by composite columns. Materials & Design. 2010;31:158-65.

[4] Li Y, Dong Y, Qin Y, Lv H. Nonlinear forced vibration and stability of an axially moving viscoelastic sandwich beam. International Journal of Mechanical Sciences. 2018;138:131-45.

[5] Jiang WZ, Liu Y, Wang B. The plastic behavior of sandwich beams with core gradation. International Journal of Mechanical Sciences. 2017;130:19-30.

[6] Xiong J, Ma L, Wu L, Wang B, Vaziri A. Fabrication and crushing behavior of low density carbon fiber composite pyramidal truss structures. Composite Structures. 2010;92:2695-702.

[7] Metwally H, Manglik RM. Enhanced heat transfer due to curvature-induced lateral vortices in laminar flows in sinusoidal corrugated-plate channels. International Journal of Heat and Mass Transfer. 2004;47:2283-92.

[8] Pandey SD, Nema V. Experimental analysis of heat transfer and friction factor of nanofluid as a coolant in a corrugated plate heat exchanger. Experimental Thermal and Fluid Science. 2012;38:248-56.

[9] Khan T, Khan M, Chyu M-C, Ayub Z. Experimental investigation of single phase convective heat transfer coefficient in a corrugated plate heat exchanger for multiple plate configurations. Applied Thermal Engineering. 2010;30:1058-65.

[10] Xu GD, Wang ZH, Zeng T, Cheng S, Fang DN. Mechanical response of carbon/epoxy composite sandwich structures with three-dimensional corrugated cores. Composites Science and Technology. 2018.

[11] Paczos P, Wasilewicz P, Magnucka-Blandzi E. Experimental and numerical investigations of five-layered trapezoidal beams. Composite Structures. 2016;145:129-41.

[12] Kooistra GW, Deshpande V, Wadley HN. Hierarchical corrugated core sandwich

panel concepts. Journal of Applied Mechanics. 2007;74:259-68.

[13] Han B, Qin K, Yu B, Wang B, Zhang Q, Lu TJ. Honeycomb–corrugation hybrid as a novel sandwich core for significantly enhanced compressive performance. Materials & Design. 2016;93:271-82.

[14] Rubino V, Deshpande V, Fleck N. The three-point bending of Y-frame and corrugated core sandwich beams. International Journal of Mechanical Sciences. 2010;52:485-94.

[15] Cheon YJ, Kim HG. An equivalent plate model for corrugated-core sandwich panels. Journal of Mechanical Science and Technology. 2015;29:1217-23.

[16] Zhang J, Supernak P, Mueller-Alander S, Wang CH. Improving the bending strength and energy absorption of corrugated sandwich composite structure. Materials & Design. 2013;52:767-73.

[17] Yang JS, Xiong J, Ma L, Feng LN, Wang SY, Wu LZ. Modal response of all-composite corrugated sandwich cylindrical shells. Composites Science and Technology. 2015;115:9-20.

[18] Wu ZJ, Li FM, Wang YZ. Vibration band gap behaviors of sandwich panels with corrugated cores. Computers & Structures. 2013;129:30-9.

[19] Pellerin RF, Ross RJ. Transverse vibration and longitudinal stress wave non-destructive evaluation methods. Nondestructive evaluation of wood Forest Products Society, Madison. 2002.

[20] Drinkwater BW, Wilcox PD. Ultrasonic arrays for non-destructive evaluation: A review. Ndt & E International. 2006;39:525-41.

[21] Shuvalov A, Poncelet O, Deschamps M, Baron C. Long-wavelength dispersion of acoustic waves in transversely inhomogeneous anisotropic plates. Wave Motion. 2005;42:367-82.

[22] Wang L, Rokhlin S. Floquet wave homogenization of periodic anisotropic media. The Journal of the Acoustical Society of America. 2002;112:38-45.

[23] Wu Q, Gao Y, Wei X, Mousanezhad D, Ma L, Vaziri A, et al. Mechanical properties and failure mechanisms of sandwich panels with ultra-lightweight three-dimensional hierarchical lattice cores. International Journal of Solids and Structures. 2017.

[24] Dong HW, Su XX, Wang YS, Zhang C. Topological optimization of two-dimensional phononic crystals based on the finite element method and genetic algorithm. Structural and Multidisciplinary Optimization. 2014;50:593-604.

[25] Veres IA, Berer T, Matsuda O. Complex band structures of two dimensional phononic crystals: Analysis by the finite element method. Journal of Applied Physics. 2013;114:083519.

[26] Wang ZP, Sun CT. Modeling micro-inertia in heterogeneous materials under dynamic loading. Wave Motion. 2002;36:473-85.

[27] Barthélémy R, Jacques N, Kerampran S, Vermeersch F. Modelling of micro-inertia effects in closed-cell foams with application to acoustic and shock wave propagation. International Journal of Solids and Structures. 2016;97:445-57.

[28] Airoldi L, Ruzzene M. Design of tunable acoustic metamaterials through periodic arrays of resonant shunted piezos. New Journal of Physics. 2011;13:113010.

[29] Hui T, Oskay C. A nonlocal homogenization model for wave dispersion in dissipative composite materials. International Journal of Solids and Structures. 2013;50:38-48.

[30] Parnell WJ, Abrahams ID. Dynamic homogenization in periodic fibre reinforced media. Quasi-static limit for SH waves. Wave Motion. 2006;43:474-98.

[31] Chen W, Fish J. A dispersive model for wave propagation in periodic heterogeneous media based on homogenization with multiple spatial and temporal scales. Journal of applied mechanics. 2001;68:153-61.

[32] Andrianov IV, Bolshakov VI, Danishevs' kyy VV, Weichert D. Higher order asymptotic homogenization and wave propagation in periodic composite materials. Proceedings of the Royal Society of London A: Mathematical, Physical and Engineering Sciences. 2008: 1181-201.

[33] Andrianov IV, Danishevs'kyy VV, Ryzhkov OI, Weichert D. Dynamic homogenization and wave propagation in a nonlinear 1D composite material. Wave Motion. 2013;50:271-81.

[34] Arabnejad S, Pasini D. Mechanical properties of lattice materials via asymptotic homogenization and comparison with alternative homogenization methods. International Journal of Mechanical Sciences. 2013;77:249-62.

[35] Mei CC, Vernescu B. Homogenization methods for multiscale mechanics: World scientific; 2010.

[36] Wu S. Classical solutions of forced vibration of rod and beam driven by displacement boundary conditions. Journal of Sound and Vibration. 2005;279:481-6.

[37] Oleinik O. On homogenization problems. Trends and applications of pure mathematics to mechanics: Springer; 1984. p. 248-72.

[38] Hassani B, Hinton E. A review of homogenization and topology optimization III—topology optimization using optimality criteria. Computers & Structures. 1998;69:739-56.

[39] Qing N, Jian-Chun C. Homogenization of two-dimensional phononic crystals at low frequencies. Chinese Physics Letters. 2005;22:2305.

[40] Graff KF. Wave motion in elastic solids: Courier Corporation; 2012.

[41] Deshpande VS, Fleck NA. Collapse of truss core sandwich beams in 3-point bending. International Journal of Solids and Structures. 2001;38:6275-305.

[42] Lou J, Ma L, Wu LZ. Free vibration analysis of simply supported sandwich beams with lattice truss core. Materials Science and Engineering: B. 2012;177:1712-6.

Figure captions

(a)
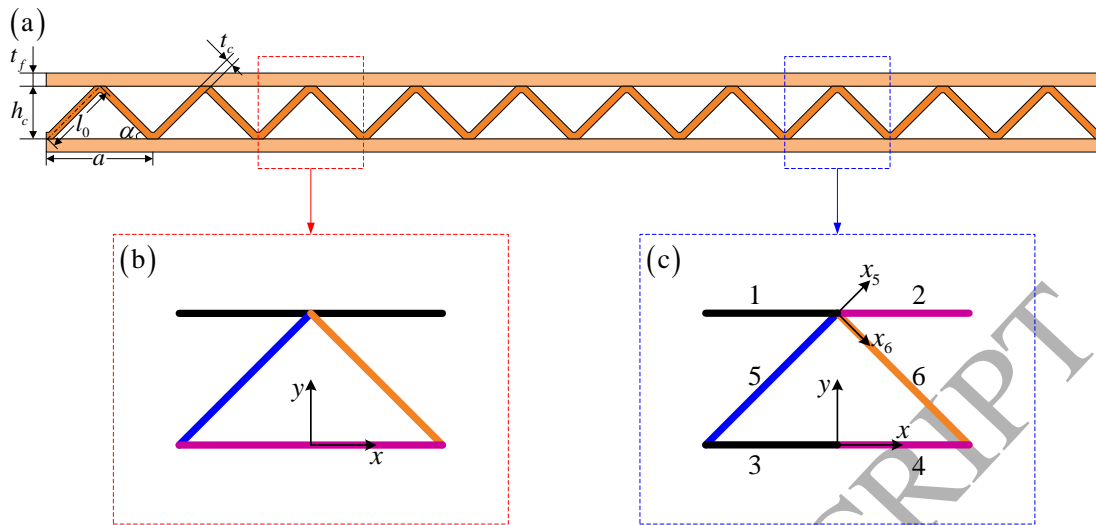
Fig.1 Sketch of an infinite long corrugated sandwich plate: (a) several unit cells; (b) a unit cell used for homogenization analysis; (c) a unit cell used for spectral element analysis
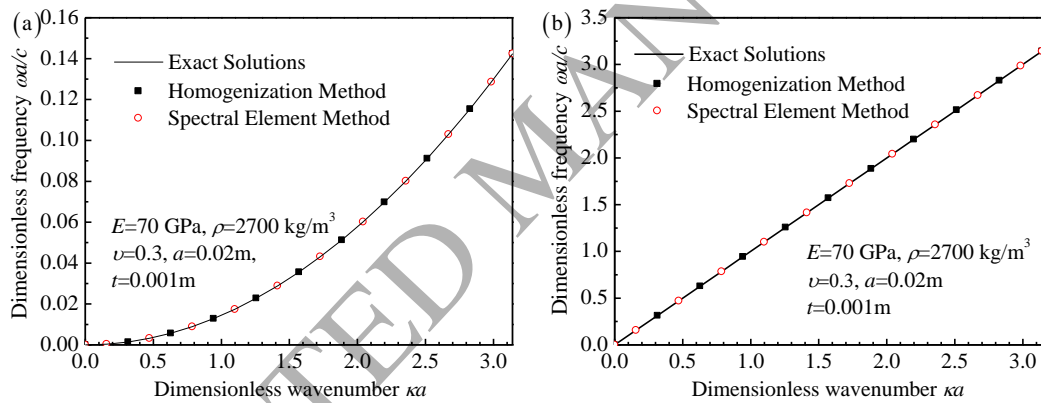
Fig.2 Dispersion curves for a homogeneous plate: (a) bending wave, (b) longitudinal wave
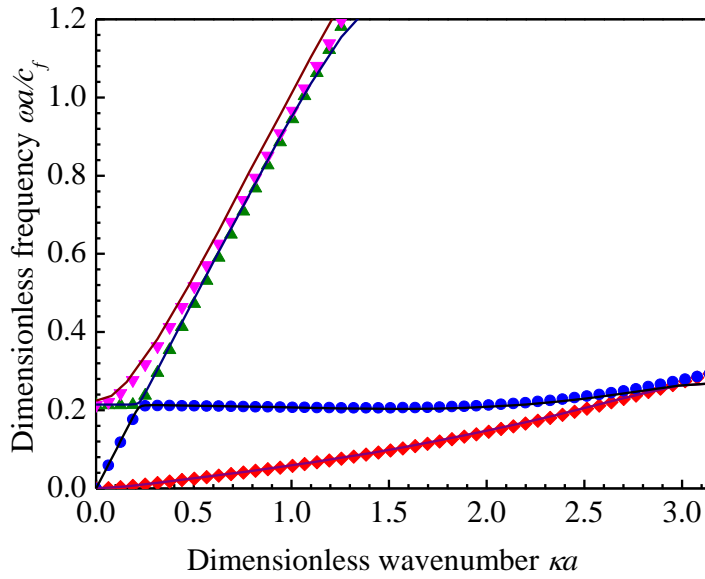
Fig.3   Dispersion curves for a corrugated sandwich plate ($\alpha = \pi/4$, dots denote the results obtained by the homogenization method, and solid lines represent those predicted by the spectral element method)
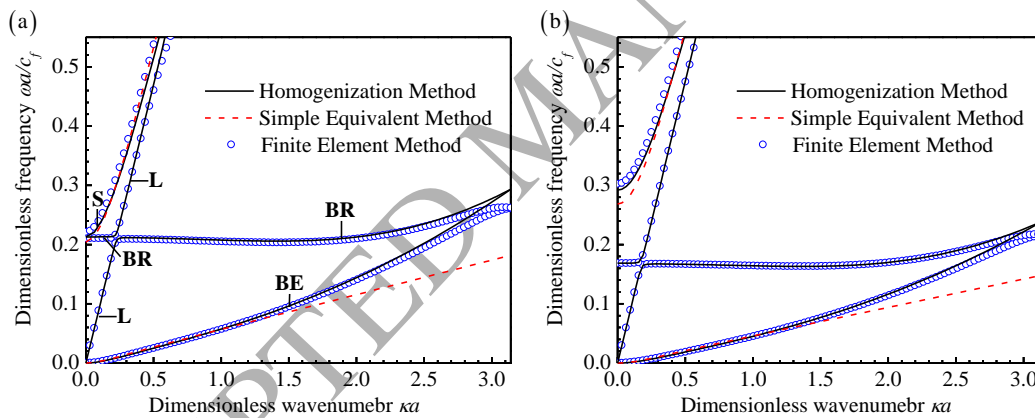
Fig.4   Dispersion curves for the corrugated sandwich plate: (a) $\alpha = \pi/4$, (b) $\alpha = \pi/6$ ('BE', 'L', 'BR' and 'S' denote corresponding wave modes, which are respectively the bending wave mode, longitudinal wave mode, breathing mode, and shear wave mode)

29
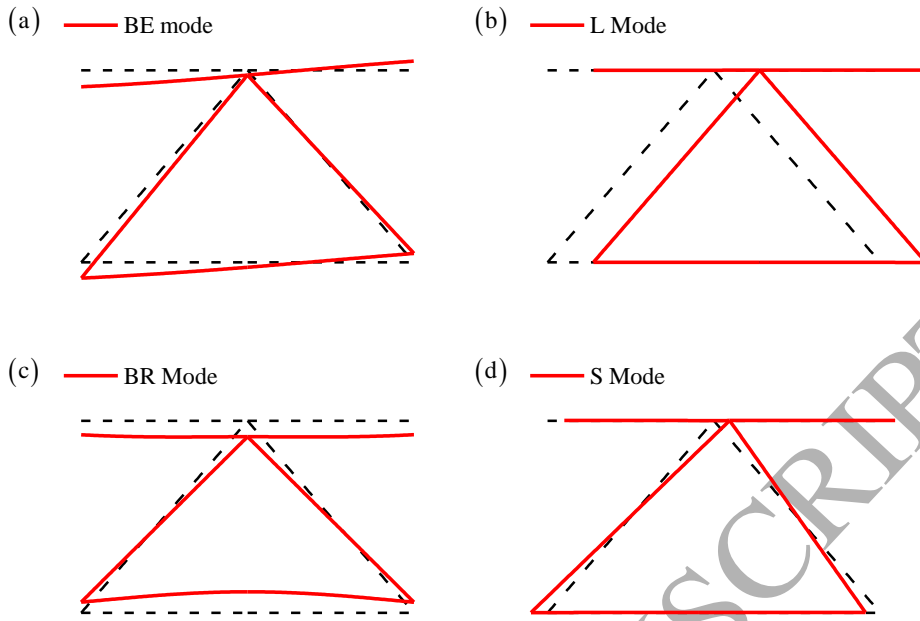
Fig.5 Wave modes of the corrugated sandwich plate ($\alpha = \pi/4$, the black dashed line depicts the reference configuration of a unit cell): (a) bending wave mode (BE mode); (b) longitudinal wave mode (L mode); (c) breathing mode (BR mode); (d) shear wave mode (S mode)
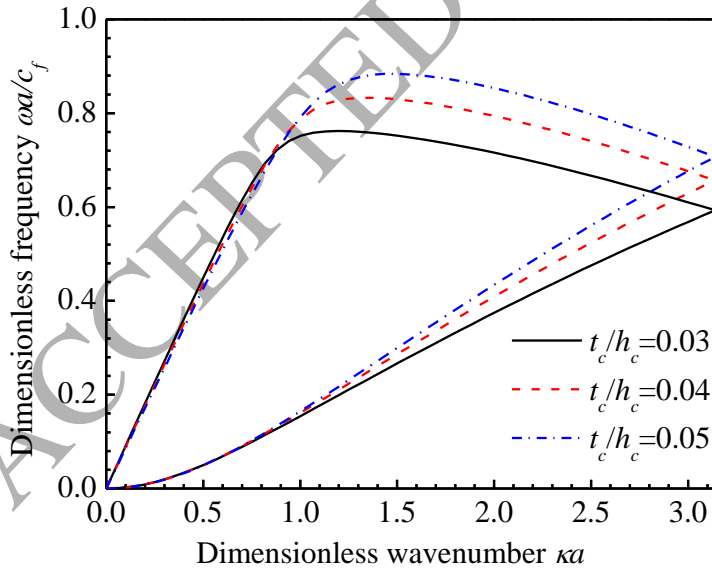
Fig.6 Effect of the thickness of the core sheets on the dispersion relations for the corrugated sandwich plate ($E_c/E_f = 1.0$, $\rho_c/\rho_f = 1.0$, $t_f/h_c = 0.10$, $\alpha = \pi/4$)
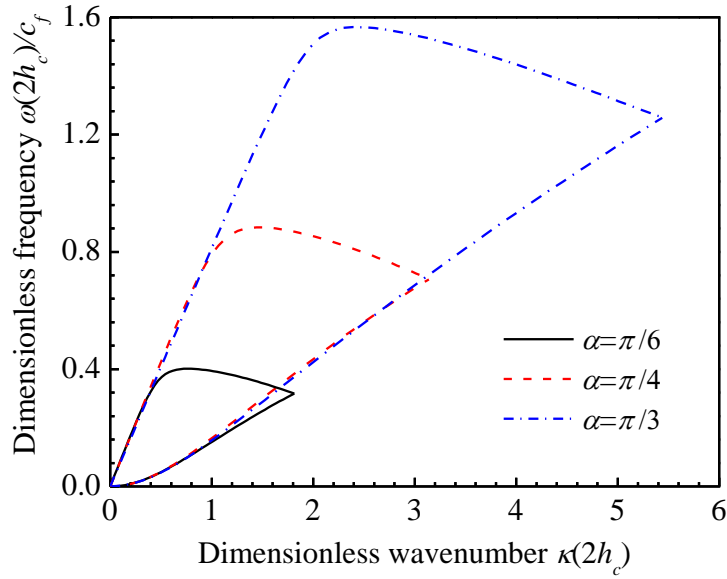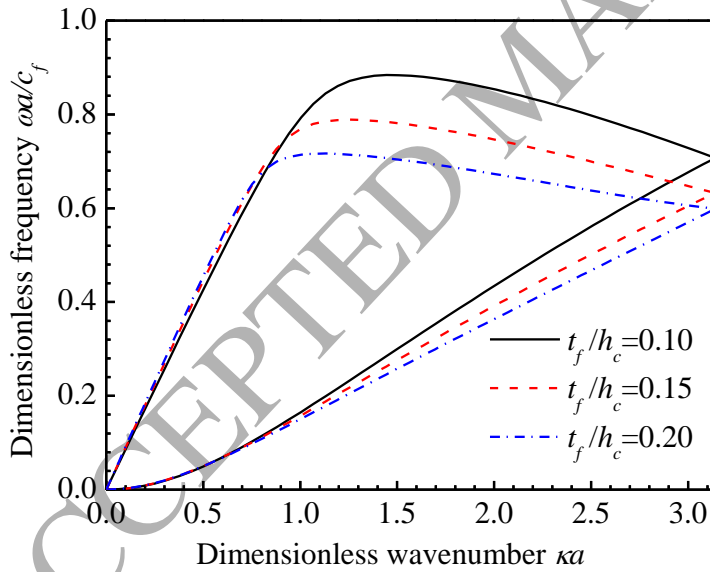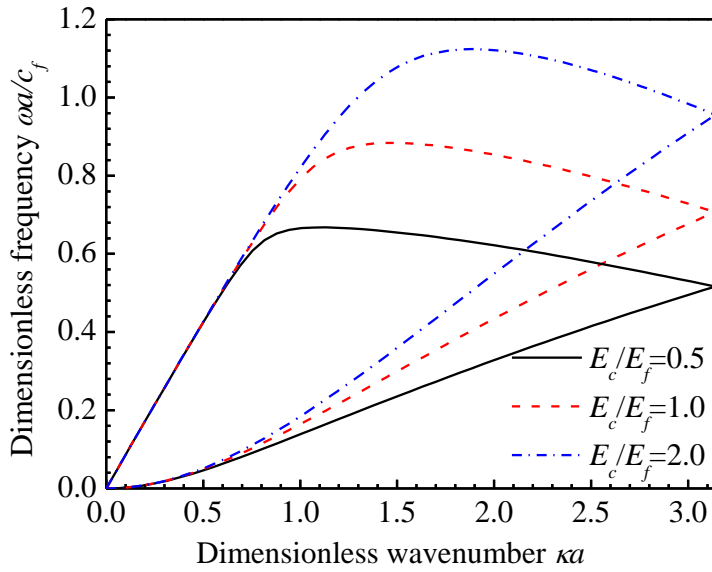
Fig.7 Effect of the inclination angle of the core sheets on the dispersion relations for the corrugated sandwich plate ($E_c/E_f = 1.0$, $\rho_c/\rho_f = 1.0$, $t_c/h_c = 0.05$, $t_f/h_c = 0.10$)

Fig.8 Effect of the thickness of the face sheets on the dispersion relations for the corrugated sandwich plate ($E_c/E_f = 1.0$, $\rho_c/\rho_f = 1.0$, $t_c/h_c = 0.05$, $\alpha = \pi/4$)

Fig.9 Effect of the Young's modulus of the corrugated core on the dispersion relations for the corrugated sandwich plate ($\rho_c/\rho_f = 1.0$, $t_c/h_c = 0.05$, $t_f/h_c = 0.10$, $\alpha = \pi/4$)
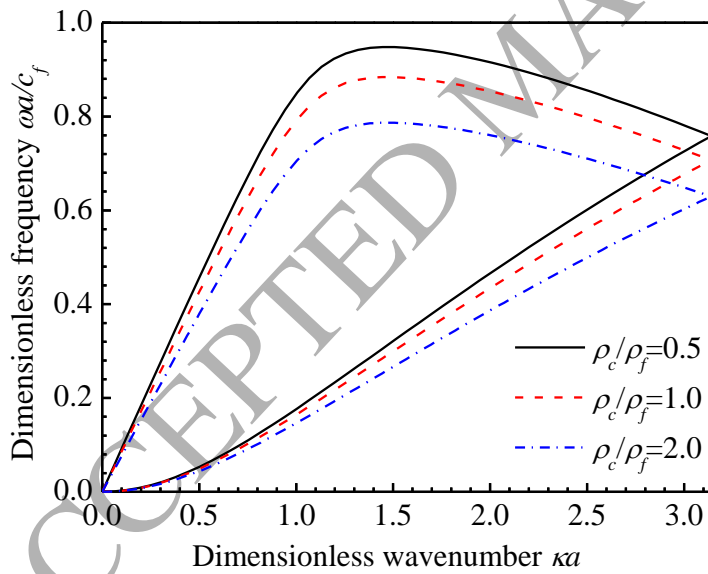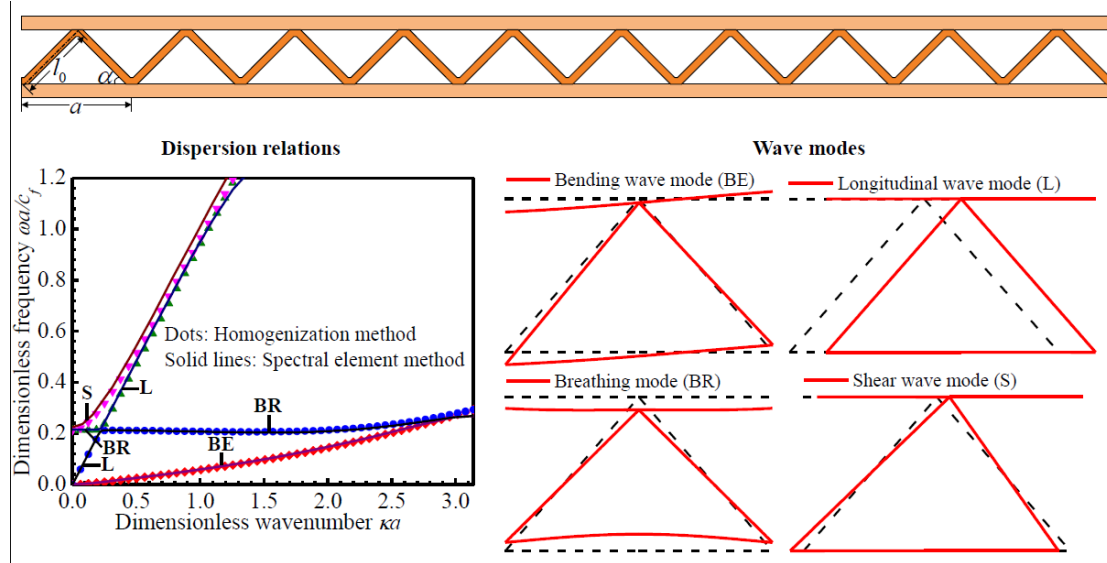

Fig.10 Effect of the density of the corrugated core on the dispersion relations for the corrugated sandwich plate ($E_c/E_f = 1.0$, $t_c/h_c = 0.05$, $t_f/h_c = 0.10$, $\alpha = \pi/4$)

GRAPHICAL ABSTRACT